PRESSURE AND STRESS ANALYSIS OF LIQUID-FILLED CYLINDRICAL TANK

Kotrasova Kamila, Kormanikova Eva and Harabinova Slavka
Faculty of Civil Engineering, Technical University of Kosice, Slovak Republic

kamila.kotrasova@tuke.sk
eva.kormanikova@tuke.sk
slavka.harabinova@tuke.sk

Abstract:

During earthquakes, the liquid-filled storage tank generates hydrodynamic pressures, in addition to hydrostatic pressure, on the solid domain of the tank. The theoretical background of hydrodynamic pressure analysis, as well as the numerical simulation of the liquid-filled cylindrical concrete tank, is the focus of this paper. The Finite Element Method (FEM) modeling, along with Arbitrary Lagrangian-Eulerian and Fluid-Structure Interactions formulation, are used for simulating the seismic response of cylindrical concrete liquid-filled tank, fixed to the rigid foundation. The Loma Prieta accelerogram is utilized for recording the seismic ground motion. In the numerical study, two states are observed: 1) static condition where only hydrostatic pressure acts, and 2) seismic excitation where hydrodynamic pressure occurs. When exposed to an earthquake situation, the tank liquid gives the total pressure of the liquid domain. The dynamic analysis considers the pressure response of the liquid domain, as well as the stress response of the solid domain of the coupled system, i.e., liquid-filled cylindrical concrete tank.

Keywords:
    Pressure, stress, tank, liquid, earthquake
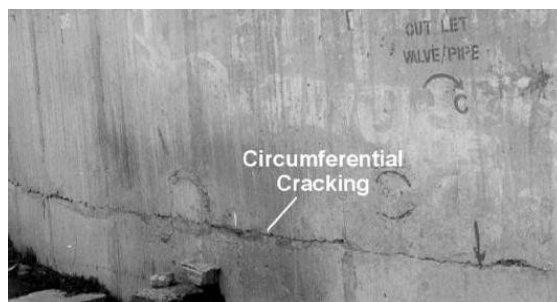
1. INTRODUCTION

Liquid storage tanks are utilized to store various types of liquids and wastes [1]. The type of storage medium, as well as the storage function of the tank, implies the design of the structure, shape, size, and the used materials [2].

Although an earthquake itself does not pose a direct danger to humans and the environment, the movement of the earth's surface can cause failure or collapse of building structures and thus have far-reaching impacts. Moreover, seismic waves can cause significant damage, disregarding the distance from the epicenter. Also, the financial damage caused by earthquakes is still rising [3]. The reason is not the increase in the frequency or intensity of the earthquakes, but primarily the growing monetary value of building materials. Earthquakes can lead to immediate damage, such as the loss of human lives and the destruction of infrastructure and property. The destruction requires rebuilding and re-creating the damaged sites, prolonging the return to standard operation [4].

FIGURE 1 Collapsed reservoir due to an earthquake [5]

The most serious is the damage to so-called "energy carriers" tanks. In the case of fire, high concentrations of toxic substances, even explosives are present [5]. They are harmful not only to the environment but also to the inhabitants of the surrounding region. The destruction (Figure 1) or even damage (Figure 2) of the reservoirs can result in contamination of the surrounding soil, ground streams, and groundwater with chemically aggressive or radioactive liquids [6].

FIGURE 2 Damage - cracks at the base of the reinforced concrete tank [5]

When designing the tank as the liquid reservoir, the integrity requirement must be satisfied even if the system is exposed to an extraordinary combination of loads. The movement of the subsoil caused by an earthquake belongs to this category. The dynamic response of liquid tanks, as well as the interaction problems of the reservoir and the stored liquid during seismic excitation, is a challenging problem of applied dynamics [7]. For predicting the behavior of the entire system, advanced computer simulations are needed. Extensive idealizations, which require a numerically substitutable model in the field of geometry, mechanical description, and material laws, must correlate with the real-life problem, so the assumptions and simplifications of the computational model are reflected in the result of the calculations [8]. In any case, the simplifications, as well as limits of numerical and computational tools used to solve the problem, must be identified.

Jacobsen [9] was presumably the first to analyze a rigid cylindrical liquid-containing tank subjected to horizontal acceleration. Housner [10] has defined the expressions for the distribution of hydrodynamic impulsive and convective pressures on the rigid cylindrical tank height, as well as tank base, exposed to the horizontal base excitation. Veletsos [9] determined the distribution of hydrodynamic pressures on the rigid and flexible circular wall. Housner [11] simplified the hydrodynamic analysis method in the tank-liquid system. Through the concept of two dynamic components, he established a spring-mass system, simulating the impulsive and convective mode of vibration for circular rigid tanks. Malhotra, Wenk, Wieland [10] determined a simple procedure for seismic analysis of flexible cylindrical liquid-storage tanks.

The use of FEM [11] was proposed as a solution to the problems of simulation of the ground-supported liquid tanks exposed to earthquakes. The fluid-structure interaction (FSI), soil-structure interaction (SSI), and sloshing of fluid are fundamental factors in the dynamic analysis of this kind of structure. Tree different finite element approaches can be used to describe the fluid motion: 1) the Eulerian approach - the potential (or pressure), is used to describe the fluid behavior [12-22], 2) the Lagrangian approach - displacement [23-31], the mixed approach - combining displacement and pressure.

The soil-structure interaction analysis contains a wide range of idealizations [30-33]. Livaoglu and Dogangun have presented the possibilities of idealization of the tank-subsoil interaction problem [34].

The knowledge of the fluid behavior, sloshing without/with roof, and sloshing impact in roofed tanks, is needed for the safety design of the tanks [35,36].

Despite the efforts to establish standards for reliable fluid reservoir design, reservoir damage still occurs today. This paper is the next contribution to this issue, providing the FEM pressure and stress analysis of a liquid-filled cylindrical concrete tank loaded with the recorded earthquake Loma Prieta accelerogram.

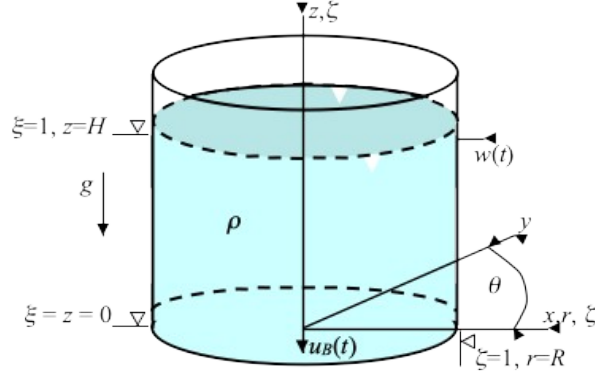## 2. SEISMIC ANALYSIS OF LIQUID-FILLED CYLINDRICAL TANKS

In a tank filled with liquid, exposed to an earthquake, the walls and the liquid charge are excited by the horizontal acceleration. The motion of the fluid within an unanchored, rigid vertical circular tanks, fixed to the foundation, can be expressed as the sum of two separate contributions:
   – the "rigid impulsive" component,
   – the "convective" load component.
The "rigid impulsive" pressure is caused by the inertia of the liquid when the rigid tank moves together with

the foundation. The boundary conditions are satisfied at the walls, as well as the bottom of the tank. However, at the fluid's free surface original position, the pressure is equal to zero, which is incorrect [37]. The "convective" pressure represents the fluid vibration in the rigid tank (sloshing). The convective pressure component satisfies the boundary conditions and the correct equilibrium condition at the free surface. The impulsive flexible pressure component emerges only in the flexible tank shell (e.g., steel tank) [12].

The cylindrical coordinate system: r, z, θ is used with origin at the centre of the tank bottom and with z vertical axis. R is the radius of liquid filling, and H is the original height of the free surface of liquid filling, see Figure 3. The mass density of the fluid is ρ, $\xi = r/R$ is dimensionless radius and $\zeta = z/H$ is dimensionless vertical coordinate [34].

FIGURE 3 Vertical cylindrical tank

2.1 Rigid impulsive component

The spatial-temporal variation of the "rigid impulsive" pressure is given by the expression

$$p_i(\xi,\zeta,\theta,t) = C_i(\xi,\zeta)\rho H \cos\theta\, A_g(t), \tag{1}$$

where

$$C_i(\xi,\zeta) = 2\sum_{n=0}^{\infty} \frac{(-1)^n}{I_1'(v_n/\gamma)v_n^2}\cos(v_n\zeta)I_1\left(\frac{v_n}{\gamma}\xi\right), \tag{2}$$

$v_n = \pi\dfrac{2n+1}{2}$ and $\gamma = H/R$, $I_1(\cdot)$ is the modified Bessel function of the order 1 and $I_1'(\cdot)$ can be expressed in

terms of modified Bessel function of order 0 and 1 $I_1'(x) = \dfrac{dI_1(x)}{dx} = I_0(x) - \dfrac{I_1(x)}{x}$. The function C_i gives the

distribution along the height of the time-dependence pressure p_i. θ is angle of circumference, $\gamma = H/R$ slenderness parameter, $A_g(t)$ the free-field ground horizontal acceleration of ground with peak value denoted by a_g. The result of an equivalent single-degree-of-freedom system is m_i with the impulsive period T_i. The distribution p_i along the height of tank wall gives the function C_i, eq. (2), for $\xi = 1$ (i.e., at the wall of the tank) and $\cos\theta = 1$ (i.e., in the plane of the horizontal seismic action).

2.2 Convective component

The spatial-temporal variation of the "convective" (sloshing) pressure component is given by the expression

$$p_c(\xi,\zeta,\theta,t) = \rho\sum_{n=1}^{\infty}\psi_n\cos(v_n\gamma\zeta)J_1(v_n\xi)\cos\theta\, A_{cn}(t), \tag{3}$$

where

$$\psi_n = \frac{2R}{(\lambda_n^2-1)J_1(\lambda_n)\cos h(\lambda_n\gamma)}, \tag{4}$$

J_1 is Bessel function of the first order, λ_n are the roots of the first-order Bessel function of the first kind (λ_1=1.8412; λ_2=5.3314; λ_3=8.5363, λ_4=11.71, λ_5=14.66 and λ_{5+i}=λ_5+5 i (i=1,2,...)). $A_{cn}(t)$ is acceleration time-history of the response of a single degree of freedom oscillator having a circular frequency ω_{cn}

$$\omega_{cn}=\sqrt{\frac{g\,\lambda_n\tan h(\lambda_n\gamma)}{R}},\qquad\qquad (5)$$

and damping ratio appropriate for the sloshing of the fluid.

Only the first oscillating or sloshing mode and frequency of the oscillating liquid (n=1) needs to be considered in expression for design purposes.

3. FINITE ELEMENT METHOD MODELING

The finite element method (FEM) is a numerical approximation method for solving the differential equations on the finite element grid. FEM was originally developed for stress and displacement analysis of structural domains. Later, the FEM has expanded into analyzing the fluids. At present, it is utilized for solving complex engineering problems involving structures, fluids, and Fluid-Structure interactions. The latter, ergo FSI, is the simulation of mechanical systems, or a fully coupled solution of fluid flows with structure interactions [15].

The mechanical principles, which govern fluids and solids are the same, but their response is quite different. These different results lead to various difficulties in numerical simulations of fluids and structures. The possibility to digitally analyze the complex interaction problems of fluid and solid domains is significant in practice. The advancements in technology, hardware, and software, enable solving the interaction problems using FEM and FSI to analyze the complex response of various combined fluid, and movable or deformable solid domains [16,17].

The FSI method is crucial for designing many engineering systems, e.g., aircraft, spacecraft, or engines and bridges. Failing to consider the effects of oscillatory interactions can be catastrophic, especially in the structures comprising materials susceptible to fatigue. Tacoma Narrows Bridge (1940) is probably one of the most infamous examples of large-scale structural failure. More common are fluid oscillations, which induce substantial forces and moments of forces on the fluid-containing transport containers' structure. That negatively affects containers' stability [18-21]. In the FSI modeling, fluid and solid domains are coupled together to produce a single result that cannot be produced when the domains are evaluated individually.

This multiphysics coupling between the laws describing fluid dynamics and structural mechanics is characterized by interactions, which can be stable or oscillatory, between a deformable or moving structure and a surrounding or internal fluid flow [22]. For the solution of fully-coupled fluids with structure interactions, three different finite element approaches representing fluid motion are possible: Eulerian (utilizes velocity potential or pressure), Lagrangian (uses displacement field), mixed methods (both, the pressure and displacement fields, are included in the element formulation) [23].

In FSI analyses, the fluid forces are applied to the solid domain, and the solid domain retroactively changes the fluid domain [24]. For most interaction problems, the computational domain is divided into fluid and solid [25]. The fluid and solid models are defined independently; through their material data, boundary conditions, etc. The interaction occurs on the interface of the two domains [26].

In many fluid flow calculations, the computational fluid domain remains unchanged in time. That is valid for problems that involve rigid boundaries. These are suitably handled with the Eulerian formulation of equilibrium equations [27]. In the case where the shape of the fluid domain is expected to change significantly, a modified formulation called Arbitrary Lagrangian-Eulerian (ALE) formulation was adopted to adequately simulate the physical behavior of the domain of interest [28]. The ALE description was designed to follow the boundary motions rather than the fluid particles. Therefore, the fluid particles flow through a moving FE-mesh.

The Lagrangian equations of motion of the structure are given by [28]

$$\rho\frac{\partial^2 u}{\partial t^2}=\nabla\cdot\tau+f^B,\qquad\qquad (6)$$

where ρ is the density, t the time, $\boldsymbol{\tau}$ the Cauchy stress tensor, $\mathbf{u}$ the vector of structural displacements, $\mathbf{f}^B$ the vector of body forces and $(\nabla\cdot)$ is the divergence operator.

The boundary conditions for solving of Eq. (6) are,

$$u=u_S\qquad\text{on }S_u$$
$$\tau\cdot n=f^S\text{ on }S_{f,}\qquad\qquad (7)$$

S_u and S_f are the parts of the boundary with prescribed displacements $\mathbf{u}_S$, and tractions $\mathbf{f}^S$, respectively. $\mathbf{n}$ represents a unit outward normal vector to the boundary.

The fluid flow equations of a compressible Newtonian fluid flow in the ALE description of motion are

$$\rho \frac{\delta v}{\delta t} + \rho\left[(v - \hat{v}) \cdot \nabla\right]v = \nabla \cdot \tau + f^B \tag{8}$$

$$\frac{\delta\rho}{\delta t} + (v - \hat{v}) \cdot \nabla \rho + \rho \nabla \cdot v = 0 \tag{9}$$

$$\rho \frac{\delta e}{\delta t} + \rho(v - \hat{v}) \cdot \nabla e = \tau \cdot D - \nabla \cdot q + q^B \tag{10}$$

where ρ is the density of liquid, $\delta/\delta t$ is the total time derivative "seen" by a probe moving with the ALE frame, τ represents the fluid stress tensor, e is the specific internal energy, q^B is the rate of heat generated per unit volume, $\mathbf{v}$ is the fluid velocity vector, $\hat{v}$ is the velocity vector of the moving ALE frame, $\mathbf{f}^B$ is the vector of fluid body forces, $\mathbf{D}$ is the velocity strain tensor given by Eq. $\left(\nabla v + (\nabla v)^T\right)/2$, $\mathbf{q}$ is the heat flux vector, $(\nabla \cdot)$ represents the divergence operator, and (∇) the gradient operator [20-21].

The moving boundaries for Eq. (3) to (5) must confirm the condition

$$\hat{u} \cdot n = \hat{u}_S \, on \, S_{\hat{u}}$$
$$\hat{u} \cdot t = \hat{u}_t \, on \, S_{\hat{u}} \tag{11}$$

where $on \, S_{\hat{u}}$ is the part of the surface with imposed displaceents $\hat{u}_S$ and $\hat{u}_t$ in the normal and tangential directions, $\mathbf{n}$ and $\mathbf{t}$ are unit normal and tangent vectors to the boundary, and $\hat{u}$ represents the boundary displacement.

The equilibrium condition at a fluid-air interface must satisfied

$$-p_0 n - \tau \cdot n = \alpha\left(\frac{1}{R_t} + \frac{1}{R_s}\right)n, \tag{12}$$

where p_0 is fluid pressure, τ is the stress tensor, $\mathbf{n}$ is a unit normal vector to interface surface, α is coefficient of surface tension between fluid and air, R_t and R_S are the principal radii of curvatures of the interface surface.

The equilibrium and compatibility conditions must be satisfied for interface between fluid flow and solid

$$\tau^S \cdot n = \tau^F \cdot n$$

$$u^I(t) = \hat{v}^I(t), \tag{13}$$

$$\dot{u}^I(t) = v^I(t) = \hat{v}^I(t)$$

$$\ddot{u}^I(t) = \dot{v}^I(t) = \hat{\dot{v}}^I(t), \tag{14}$$

where $\mathbf{n}$ is unit vector normal to the fluid-solid interface, $\mathbf{u}$ the displacements of the structure, $\hat{u}$ the displacements of the fluid domain, $\mathbf{v}$ the fluid velocity, $\hat{v}$ the velocity of the fluid domain. The dot represents a time derivative. The superscripts I, S and F denote interface, solid and fluid media respectively [3,24].

The coupled FSI equations using FEM are

$$A\ddot{U} + B\dot{U} + CU = G \tag{15}$$

where $\mathbf{A}$ represents the mass matrix, $\mathbf{C}$ represents the tangent coefficient matrix, the matrix $\mathbf{B}$ contains the mass and tangent coefficient members, the vector $\mathbf{G}$ represents the externally applied forces, $U, \dot{U}$, and $\ddot{U}$ represent the vectors of nodal displacements, nodal velocities, and nodal accelerations, respectively.
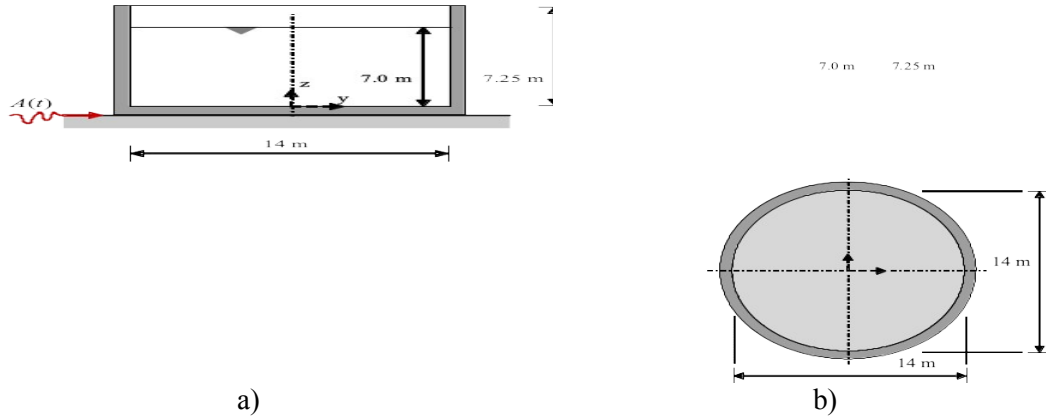
The complete system is divided into two separated subsystems, the fluid and the solid domain (structure). The coupled FSI system is calculated using the already developed fluid flow and structural solvers. The solution of one domain is separated from the solution of the other one. The iterations between both domain equations are each time of the load step.

4. NUMERICAL ANALYSIS

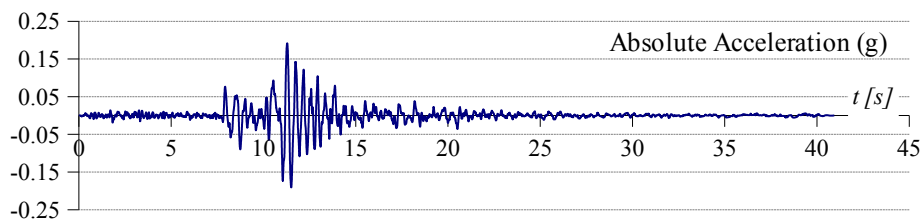The ground supported reinforced concrete open-top cylindrical tank is considered in Figure 4.

The material characteristics of tank solid domain are: Young's modulus $E = 3.4 \cdot 10^9$ N·m^{-2}, Poisson ratio $\nu = 0.2$ and volumetric mass density $\rho = 2540$ kg·m^{-3}.

The material characteristics of the liquid filling domain (water - H_2O) are bulk modulus $B = 2.1 \cdot 10^9$ N·m^{-2} and volumetric mass density $\rho_w = 1\,000$ kg·m^{-3}.

a)   b)

FIGURE 4 The tank geometry, a) vertical section, side view, b) horizontal section, top view
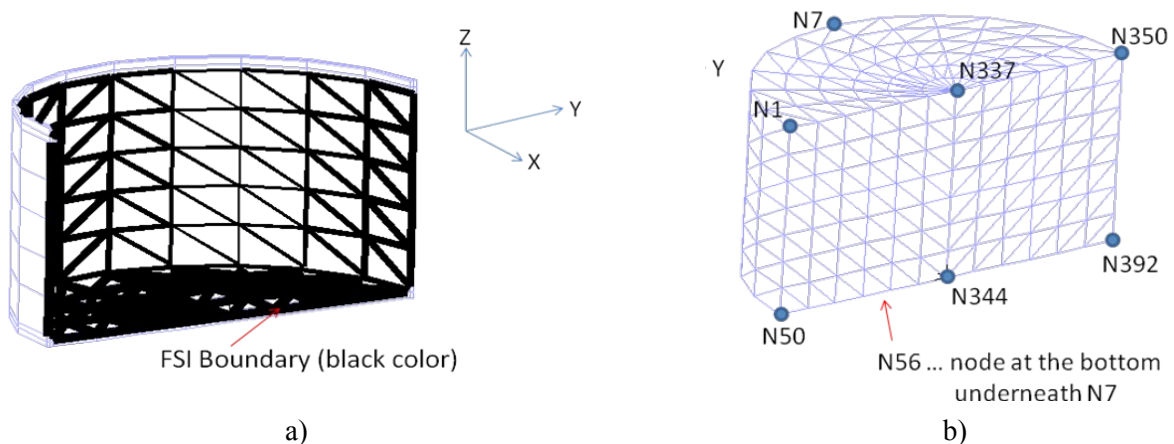
The accelerogram of the earthquake in Loma Prieta (California, 18.10.1989) was, in the numerical analysis, considered for the seismic loading only in the horizontal y – direction (Figure 5).

FIGURE 5 The accelerogram Loma Prieta, California

The dynamic time-history response of the concrete cylindrical fluid tank was realized through the numerical simulation utilizing the finite element method (FEM). The numerical model represents two separate computational domains that are bounded by the corresponding binding conditions. To solve this problem, the Lagrange-Eulerian formulation (ALE) was applied. The solid domain, representing the walls and the base of the cylindrical container, was modeled as a flexible structure with linear material and geometric properties of the 3D SOLID finite elements. The calculations of the deformations and the stresses were performed by the classic FEM deformation formulation (Figure 6a). The fluid domain of the liquid filling of the cylindrical container was modeled as an incompressible fluid, using the 3D FLUID finite elements. The fluid's velocity and pressure were obtained by solving the Navier-Stokes equations, respecting the before-mentioned assumptions (Figure 6b). The separately-defined fluid domain was considered as fully interacting with the structure's solid domain. The reciprocal liquid-structure interaction techniques (FSI) were used to simulate the structure-liquid interactions at their common boundary; the FSI boundary is showed in the black color in Figure 6a.
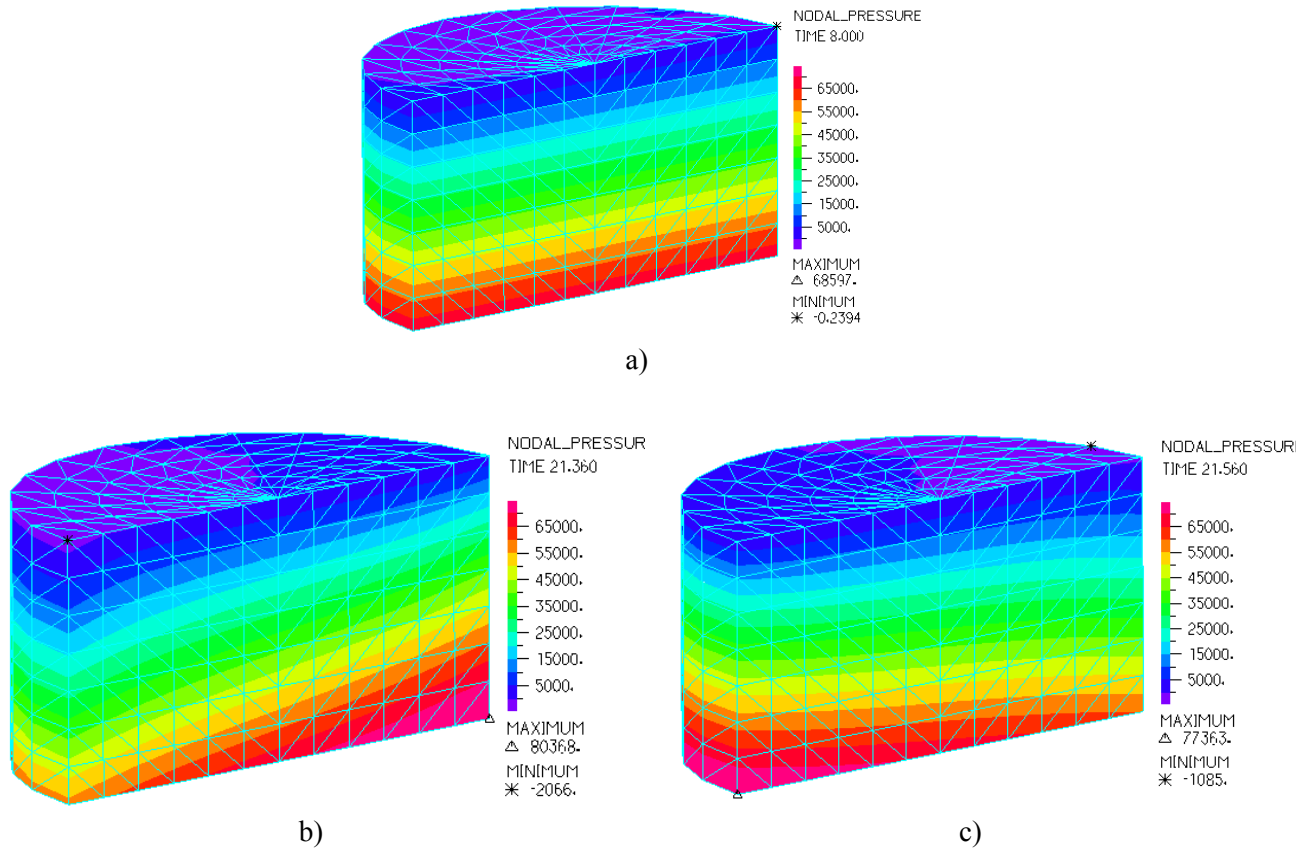
The numerical simulation of the problem simulated the quiescent state of the liquid-filled tank for the first 10 seconds, employing hydrostatic analysis. The seismic loading began to act after 10 seconds to analyze the dynamic, time-dependent response of the liquid-filled tank.
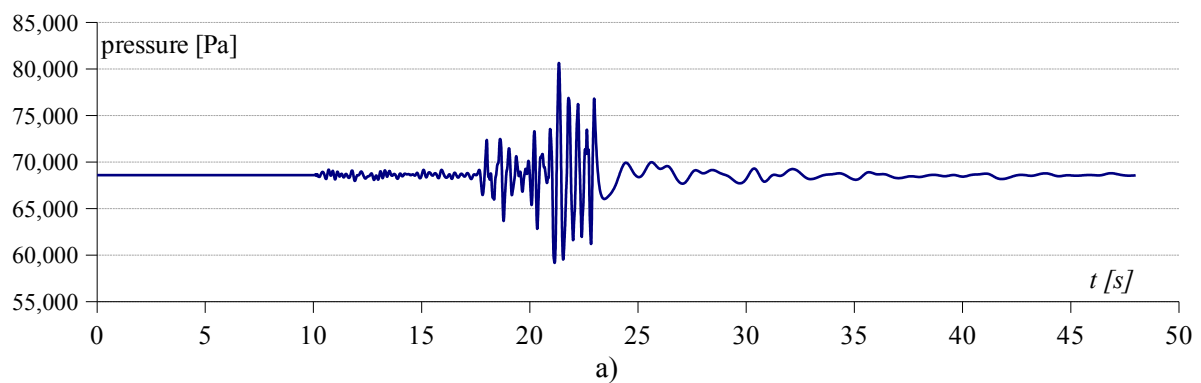

a)   b)

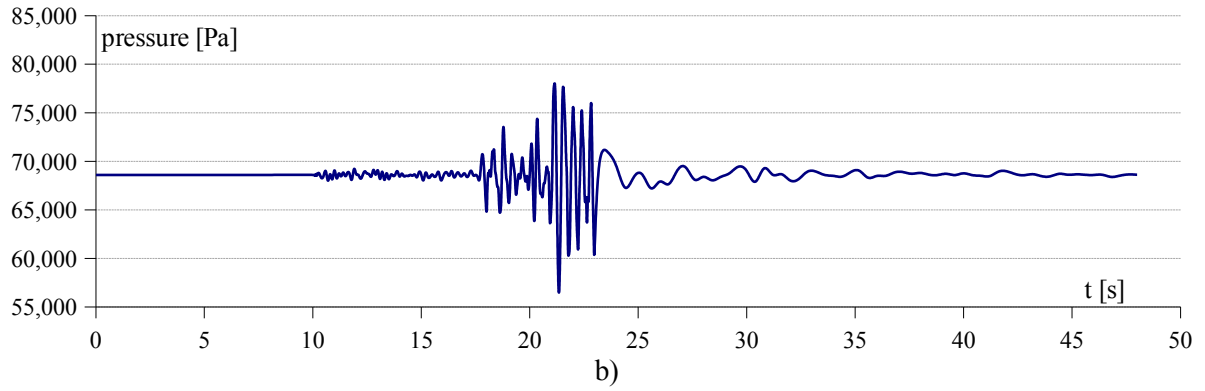**FIGURE 6** FE model of liquid-filled cylindrical tank, a) the solid domain with FSI boundary, b) fluid domain

5. RESULTS AND DUSCUSSION

Figure 7 presents the pressure distribution in the liquid domain. Figure 7a documents the pressure distribution of the liquid in time 8.0 s. The domain is in a quiet condition (i.e., before the seismic loading) with only gravity load acting on the liquid. The peak value of liquid hydrostatic pressure is 68.597 kPa and arises at the bottom of the liquid domain. Figure 7b shows the total pressure distribution in the liquid domain at 21.36 s, the time of the peak response of fluid pressure. The peak value of liquid pressure is 80.368 kPa, which arises in node 392. The liquid pressure distribution of the liquid domain at 21.56 s is documented in Figure 7c, with the peak response of fluid pressure of 77.363 kPa in node 50.

a)

b)   c)

FIGURE 7 The pressure of the liquid domain, a) in time 8 s, b) 21.36 s, c) 21.56 s
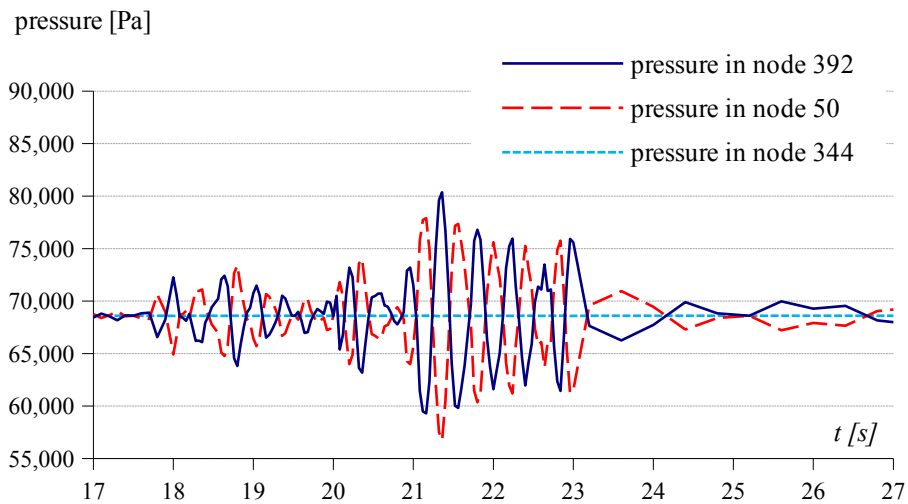
a)

FIGURE 8 Time-dependent response of the liquid pressure in the node 392 (a) and 50 (b)

The resulting time-dependent responses of the pressure of the liquid-containing cylindrical concrete tank were presented in Figures 8-10. Figure 8 documents the time-dependent response of the liquid pressure in nodes 392 (Figure 8a), and 50 (Figure 8b) at each step of the simulation. The constant liquid domain pressure of 68.597 kPa arises in the "quiet condition". It is in time 0 - 10 s, where only hydrostatic pressure of liquid acts. It correlates with the analytical result of hydrostatic pressure: $p = \rho \cdot g \cdot h = 1000 \cdot 9.81 \cdot 7.0 = 68.67$ kPa.
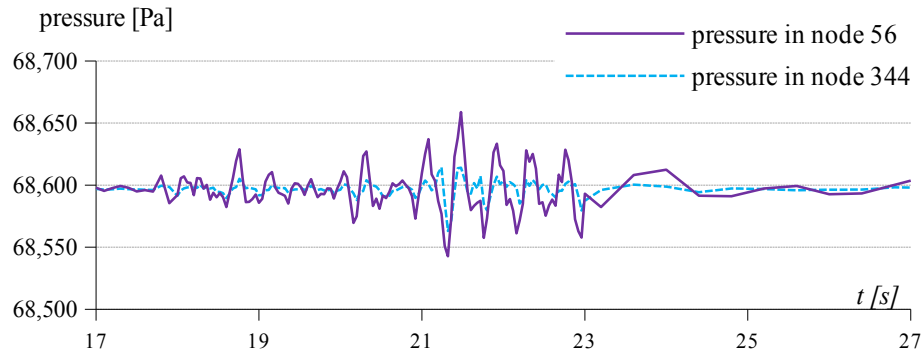
The seismic loading starts after the first 10 s of the quiet condition and excites the cylindrical liquid-filled tank by the 38 s long record of accelerogram Loma Prieta. The peak response of liquid pressure of 77.363 kPa arises in the 21.36 s, ergo the time when the seismic loading acts. Node 392 is a bottom-right node of the liquid filling domain, and node 50 is a bottom-left node of the liquid filling domain; see Figure 6b. The timing of the time-dependent response correlates well with the Loma Prieta earthquake.

Figure 9 shows the comparison of resulting time-dependent responses of the liquid pressure within the time interval of 17-27 s in the nodes 392, 50, and 344. The nodes 392, 50, and 344 are situated at the bottom of the liquid filling domain, in the *y*-axis direction. It is observed that the time-dependent responses of the liquid pressure in node 392 (bottom-right edge node of the liquid domain) and 50 (bottom-left edge node of the liquid domain) are almost asymmetric.

The time-dependent response of the liquid pressure within the examined time interval of 17-27 s in nodes 56 and 344, is described in Figure 10. The nodes are situated in the *x*-axis direction, at the bottom of the liquid domain.

FIGURE 9 Time-dependent response of the liquid pressure in nodes 392, 50 and 344
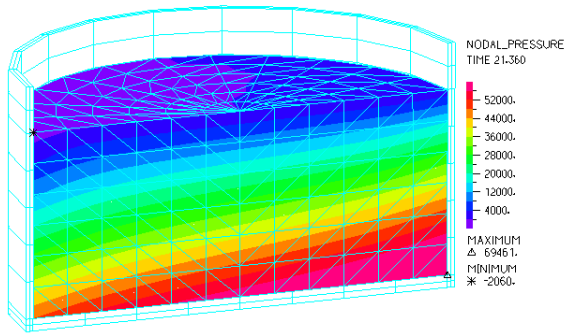
FIGURE 10 Time-dependent response of the liquid pressure in nodes 56 and 344
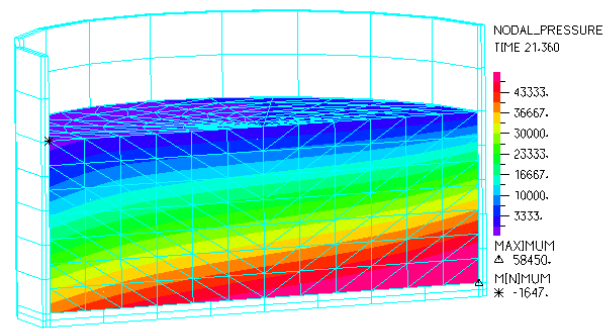
Figure 11 presents the shape and pressure distribution of fluid domain in time 21.36 s - the time of peak values of liquid pressures:

    a) for the height of liquid filling 6.0 m,
    b) for the height of liquid filling 5.0 m,
    c) for the height of liquid filling 4.0 m,
    d) for the height of liquid filling 3.0 m,
    e) for the height of liquid filling 2.0 m, and
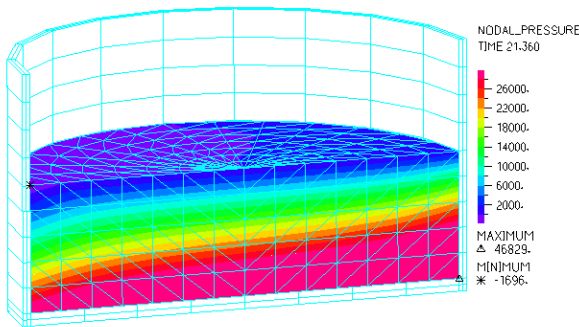   f) for the height of liquid filling 1.0.

The shape of the fluid domain is shown together with the schematically-presented solid domain of storage structure – (tank) for a better indication of the tank filling.
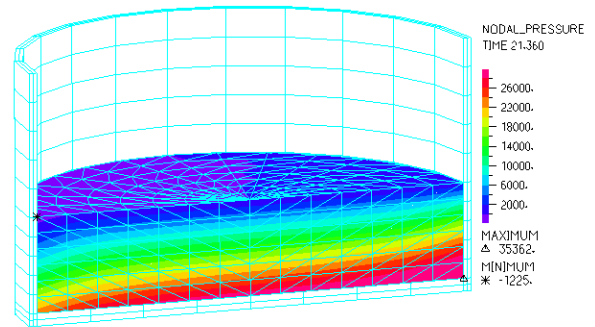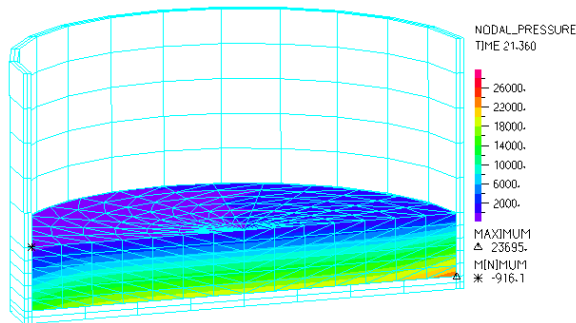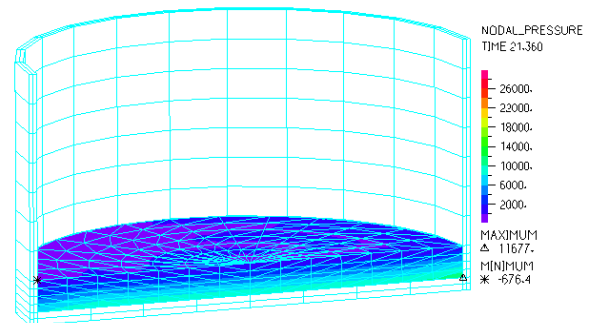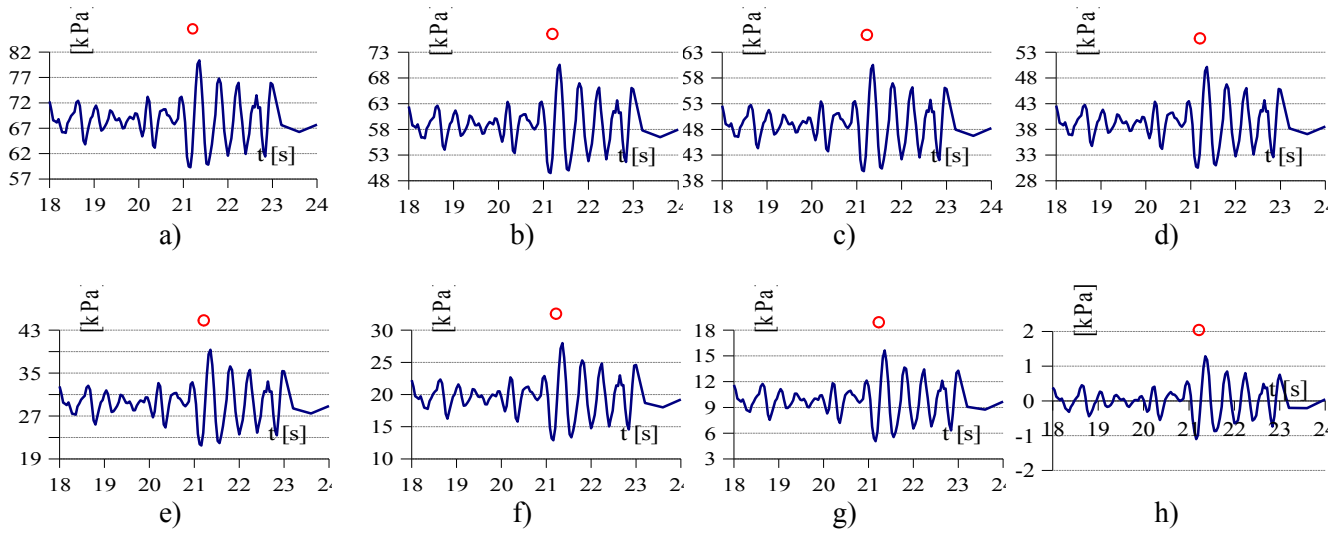

a)

b)

c)

d)

e)

f)

FIGURE 11 The liquid pressure distribution by heights of liquid filling of cylindrical tank a) 6.0 m, b) 5.0 m, c) 4.0 m, d) 3.0 m, e) 2.0 m, and f) 1.0 m
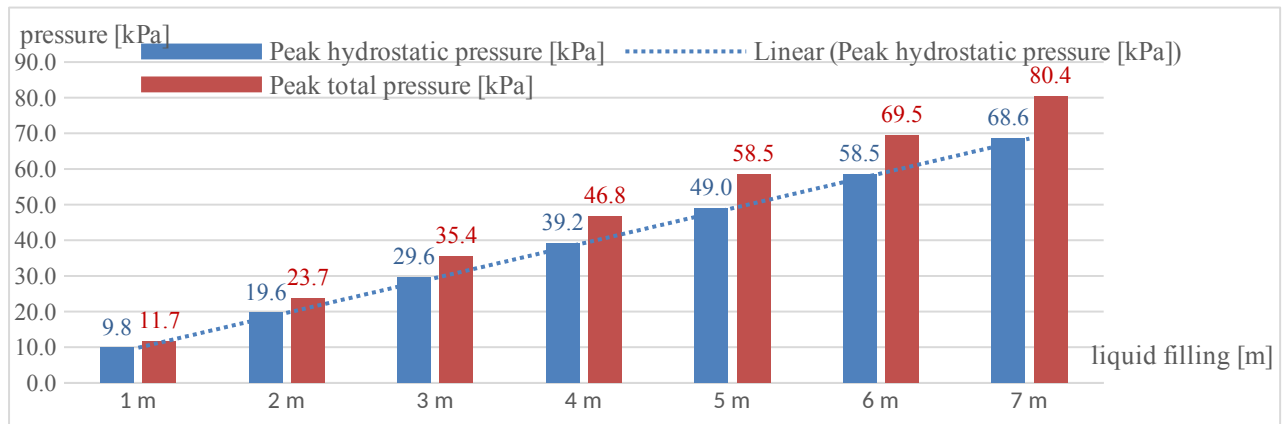
FIGURE 12 The time-dependent response of the liquid total pressure within the time interval 18-24 s in individual nodes, a) node 392, b) 386, c) 380, d) 374, e) 368, f) 362, g) 356, g) 350

The time-dependent response of the liquid total pressure between nodes 392 and 350, is documented in Figure 12:

  a) for node 392, it is the node at the bottom of fluid domain, see Fig. 6b,
  b) for node 386, it is the node 1 m up from node 392,
  c) for node 380, it is the node 2 m up from node 392,
  d) for node 374, it is the node 3 m up from node 392,
  e) for node 368, it is the node 4 m up from node 392,
  f) for node 362, it is the node 5 m up from node 392,
  g) for node 356, it is the node 6 m up from node 392,
  h) for node 350, it is the node 7 m up from node 392, see Figure 6b.

The time-dependent response of the total pressure of the liquid (Figure 12) is presented in the time interval of 18-24 s, when the time of the most evident changes in the liquid pressures, as well as the peak values of total pressures, occur in the liquid domain. It is observed that, although the pressure changes are similar, the pressure values have different total pressure oscillation intervals, which are smaller with decreasing height of the liquid filling. Red circles show the peak value of the total pressure in specific nodes.

The comparison of the peak value of the liquid pressures is presented in Figure 13. The blue columns depict the peak hydrostatic pressure values, while the red columns the peak total pressure values of the liquid domain. The peak hydrostatic pressure values are linearly growing with the increasing filling height. The values of the peak total pressure of the liquid domain are slightly higher compared to the peak hydrostatic pressure values. The highest difference of 21.4 % is perceived in the 4 m liquid filling. The percentage increase of the peak value of total liquid pressures opposite to the peak hydrostatic pressure values, for considered filling heights, are in the range of 18 % to 21.4 % (19.2 % for 1 m filling level, 20.8 % for 2 m filling, 20.2 % for 3 m filling, 19.5 % for 5 m filling, 18.0 % for 6 m filling, 17.2 % for 7 m filling).
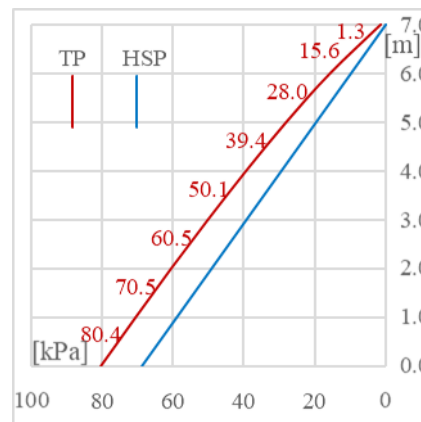
FIGURE 13 The comparison of the peak pressure depending on the liquid filling
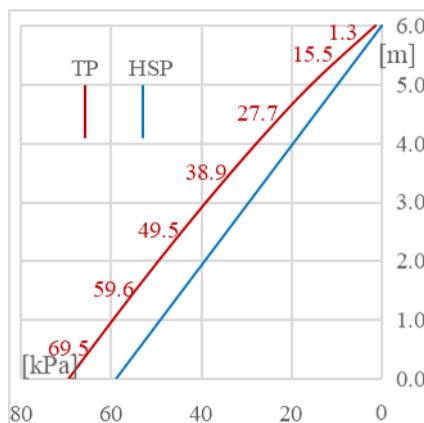
The comparison of the peak hydrostatic pressure (HSP) and the total pressure (TP) is shown in Figure 14. The peak total pressure occurs on the right side of the fluid domain at nodes aligned in a row above each other.

Fig. 14a documents the hydrostatic pressure and total pressure for the height of the liquid filling of 7.0 m, Fig. 14b for 6 m, Fig. 14c for 5 m, Fig. 14d for 4 m, Fig. 14e for 3 m, Fig. 14f for 2 m, and, finally, Fig. 14g for 1 m.
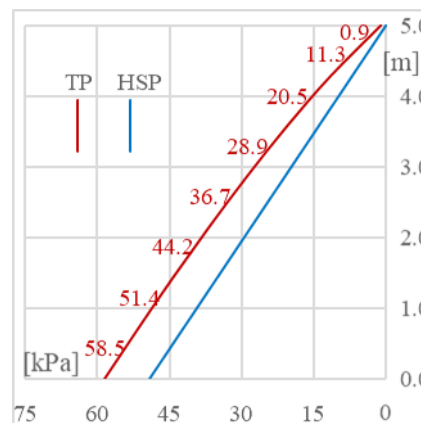
The blue linear line represents the values of the hydrostatic pressure diagrams. The red line represents the peak value of the total liquid pressure diagram throughout the numerical simulation. The hydrodynamic pressures are given zero values at the original level of the free liquid surface. Nevertheless, the peak total liquid pressure does not have a zero value at the original level, see Figure 14. The used values of the peak total pressure for 7.0 m levels of the fluid filling are documented in Fig. 12 (red circles). The values of the peak total pressure have an increasing tendency with the rising liquid level.
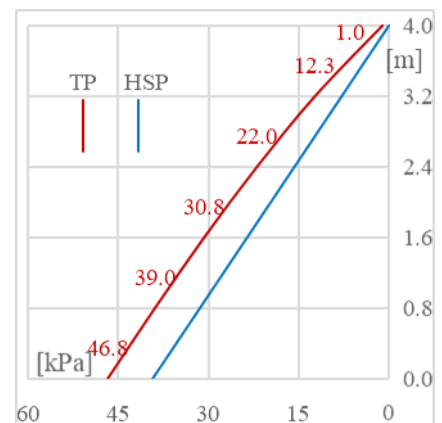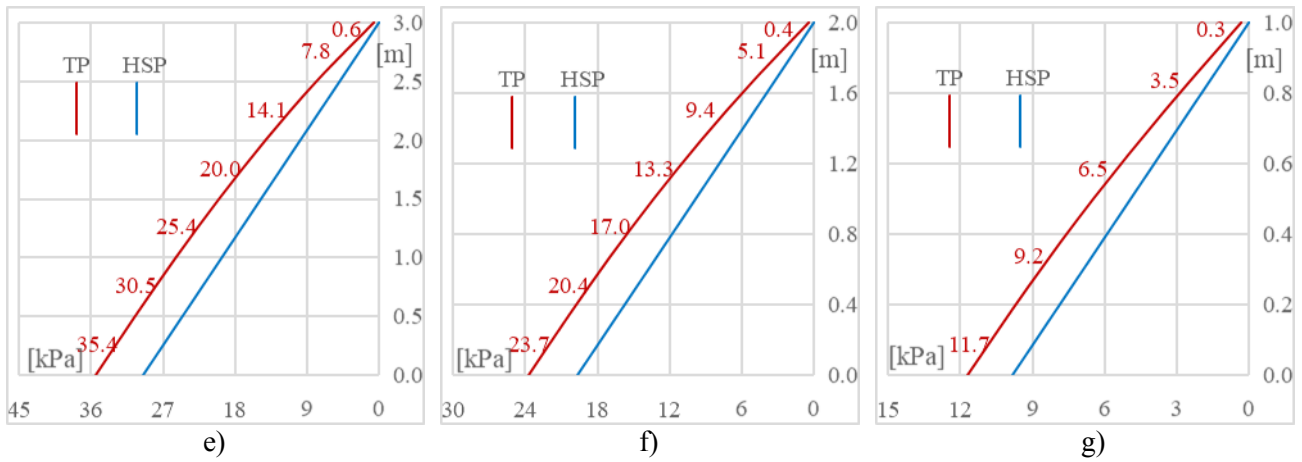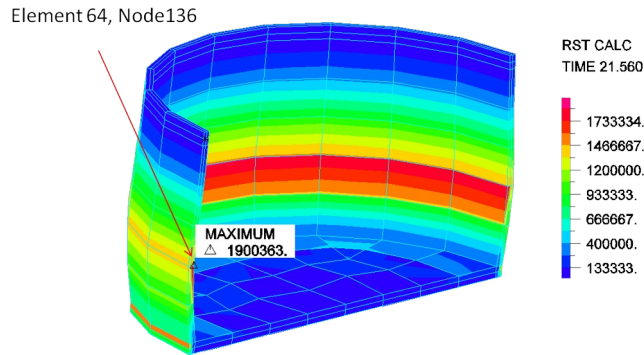

a)

b)

c)

d)

e)   f)   g)

FIGURE 14 The comparison of the peak hydrostatic pressure and the total pressure on the right side of the liquid domain, a) for 7 m filling level, b) for 6 m filling level, c) for 5 m filling level, d) for 4 m filling level, e) for 3 m filling level, f) for 2 m filling level, g) for 1 m filling level

Von Mises stress in the solid domain of the cylindrical tank with the height of the liquid filling of 7.0 m was displayed in Figure 15. The maximum Von Mises stress equals 1.9 MPa and arises in node 136, the finite element 64 in 21.56 s.

Table 1 presents the peak values of Von Mises stress during the earthquake, and the percentage increase of the peak values of Von Mises stresses relative to the Von Mises stresses from the static analysis, depending on the height of liquid filling.

FIGURE 15 Von Mises stress in time 21.56 s

TABLE 1 The peak values of Von Mises stress given during earthquake, and percentage increase of peak values of Von Mises stresses relative to the values of Von Mises stresses from the static analysis depending on height of liquid filling.

Height of liquid filling[m]	1	2	3	4	5	6	7
The peak tank Von Mises stresses – seismic effect [MPa]	0.2499	0.4011	0.6382	0.9282	1.2535	1.6152	1.9004
Percentage increase of peak tank total Von Mises stresses [%]	10.6	9.8	9.3	9.1	9.1	10.0	10.0

6. CONCLUSIONS

The ground-supported liquid-filled cylindrical tank was analyzed using the FEM - ALE FSI formulation. The tank was excited by the earthquake of Loma Prieta in California. This paper summarizes the results of the statical and seismic analysis of a liquid-filled cylindrical concrete tank. The following observed responses were of interest: the pressure of the fluid domain and stress of the solid domain. The numerical study was performed in two stages: a) the quiet condition where only hydrostatic pressure acts (0 – 10 s), and b) the seismic exciting where the hydrodynamic pressure acts together with the hydrostatic pressure, so the liquid gives the total pressure of liquid domain, observed in time 10 – 48 s. The resulting time-dependent response of the total liquid

pressure in characteristic nodes was documented throughout the 48 s of the numerical simulation. The comparison of the time-dependent response of the liquid pressure in more characteristic nodes within the interval 17 – 27 s and 18 – 24 s was performed. The full, as well as partial filling of the tank, was studied. The results were documented, and the percentage was compared, summarizing the following conclusions:

- the peak values of pressure acting on the tank wall were located at the bottom of the tank,
- the time-dependent response of the total liquid pressure in characteristic nodes was realistically documented in the quiet condition and the seismic excitation,
- the peak values of the hydrostatic pressure correlate with the analytical results of hydrostatic pressure given by $p = \rho \cdot g \cdot h$,
- the peak value of the total pressure on the tank wall was located at the bottom of the tank and resulted in greater values during the quiet condition,
- the peak value of the total pressure resulted in nonzero values in the original level of the free surface,
- the values of the peak total pressure have an increasing tendency at the original level of free surface with the increasing liquid level,
- the comparison of the time dependent response of the liquid pressure in more nodes confirms similarity of history of results with seismic loading. the comparison of the time-dependent response of the liquid pressure in more nodes confirms the similarity with the history of seismic loading results.

The presented mathematical modeling of the ground-supported liquid-filled cylindrical concrete tank subjected to seismic loading gives intriguing results for the next applied research.

REFERENCES

[1] Introduction to Storage Tanks, http://www.wermac.org/equipment/storage_tanks_vessels_general.html

[2] Batchelor GK. An introduction to fluid dynamics. Cambridge: Cambridge University Press. 1967.

[3] Kralik J, Kralik J jr. Probability assessment of analysis of high-rise buildings seismic resistance, Advanced Materials Research 2013 712-715;929-936.

[4] Safari M. Analytical Solution of Two Model Equations for Shallow Water Waves and their Extended Model Equations by Adomian's Decomposition and He's Variational Iteration Methods. WSEAS Transactions on Mathematics 2013 12 (1);1-16.

[5] Rai DC. Seismic retrofitting of R/C shaft Support of elevated tanks. *Earthquake Spectra*. 2002;(18):745-760.

[6] Kotrasová K, Kormaníková E. The study of seismic response on accelerated contained fluid. *Advances in Mathematical Physics*. 2017 (2017), p. 1-9.

[7] Dogangun A, Livaoglu R. A comparative study of the seismic analysis of rectangular tanks according to different codes. In: The 14th world Conference on Earthquake Engineering. China. 2008.

[8] Melcer J. Dynamic response of a bridge due to moving loads. Journal of Vibrational Engineering and Technologies, vibration engineering & technologies 2015 3(2);199-209.

[9] Jaiswal OR, Rai DC, Jain SK. Review of code provision on design seismic forces for liquid storage tanks. IITK-GSDMA-EQ01-V1.0. Kanpur, Indian Institute of Technology Kanpur.

[10] Housner GW. Earthquake pressures on fluid containers. California institute of technology, Pasadena California, 1954.

[11] Di Carluccio A, Fabbrocino G, Salzano E, Manfredi G. Analysis of pressurized horizontal vessels under seismic excitation. In: ICSV1 18th The World Conference on Earthquake Engineering, 2008, Beijing, China.

[12] Cherif SMH, Quissi MN. Free vibration Analysis of a Liquid in a Cylindrical rigid tank using the Hierarchical Finite Element Method. Lat. Am. J. solids struct. 2016 (13)7,1265-1280.

[13] Močilan M, Žmindák M, Pastorek P. Dynamic analysis of fuel tank. *Procedia Engineering*. 2016;(136):45-49. DOI: 10.1016/j.proeng.2016.01.172.

[14] Frei S, Richter T, Wick T. Eulerian techniques for Fluid-structure interactions – Part I: Modeling and Simulation. http://www.thomaswick.org/links/FrRiWi14_enumath_part_I.pdf

[15] Bathe KJ, Zhang H, Wang MH. Finite Element Analysis of incompressible and compressible fluid Flows with free surfaces and structural interaction. Computer & Structures 1995 56(2/2);193-213.

[16] Michalcova V, Lausová L.Numerical approach to determination of equivalent aerodynamic roughness of industrial chimneys. *Computers and Structures*.2017;(207):187-193. DOI: 10.1016/j.compstruc.2017.03.013.

[17] Chegini AHN, Pender G. Determination of Small Size Bedload Sediment Transport and its Related Bedform under Different Uniform Flow Conditions. WSEAS Transactions on Environment and Development 2018 8(4);158-167.

[18] Bathe KJ, Zhang H. Finite Element developments for general fluid flows with structural interaction. International journal for numerical methods in engineering 2004.

[19] Rugonyi S, Bathe KJ. On Finite Element Analysis of Fluid Coupled with Structural Interaction. CMES 2001 2(2);195-212.

[20] Manual ADINA. 71 Elton Ave. Watertown. MA 02472. USA. ADINA R&D. Inc. October 2005.

[21] Kotrasova K, Grajciar I. Dynamic Analysis of Liquid Storage Cylindrical Tanks Due to Earthquake. Advanced Materials Research 2014 969;119-124.

[22] Kotrasova K, Kormanikova E. A case study on seismic behavior of rectangular tanks considering fluid - structure interaction. International Journal of Mechanics 2016 10;242-252.

[23] Zienkiewicz O, Bettess P. Fluid-Structure Dynamic Interaction and Wave Forces. An introduction of Numerical Treatment. Inter. J. of Num. Meth. 1978 (13), 1-16.

[24] Savio De Goes Maciel E. TVD and ENO Applications to Supersonic Flows in 3D – Part II. WSEAS Transactions on Fluid Mechanics 2013 8 (1).

[25] Jacobs GB, Don WS, Dittmann T. High-order resolution Eulerian–Lagrangian simulations of particle dispersion in the accelerated flow behind a moving shock. Theoretical and Computational Fluid Dynamics 2012 26(1);37-50.

[26] Jendzelovsky N, Balaz L. Numerical Modeling of Cylindrical Tank and Compare with Experiment. Applied Mechanics and Materials 2014 617;148-151.

[27] Bathe KJ, Zhang HS. Finite Element Analysis of fluid Flows with structural interactions. Computer & Structures 1999 72(2/2);1-16.

[28] Cherif SMH, Ouissi MN. Free vibration analysis of a liquid in a circular cylindrical rigid tank using hierarchical Finite element method. Latin American Journal of Solid and Structures 2016 13(7);

[29] Kock E, Olson L. Fluid-structure interaction analysis by the finite element method a variational approach. International Journal for Numerical Methods in Engineering 1991 31(3);463-491.

[30] Wang X. Fundamentals of Fluid – Solid Interactions. Analytical and Computational Approaches. Elsevier. Linacre House. Oxford OX2 8DO. UK. 2008.

[31] Kotrasova K, Grajciar I, Kormanikova E. A Case Study on the Seismic Behavior of Tanks Considering Soil-Structure-Fluid Interaction. Journal of vibration engineering & technologies 2015 3(3);315-330.

[32] Dago NO. Geotechnical subsoil investigation for the design of water tank foundation. International journal of sciences and research publications. 20014 4(3), 1-10.

[33] Ye J, Jeng D, Wang R, Zhu C. A 3-D semi-coupled numerical model for fluid-structures-seabed-interaction (FSSI-CAS 3D): Model and verification. Journal of fluids and structures. 2013 (40), 148-162.

[34] Livaoglu R, Dogangun A. Simplified seismic analysis procedure for elevated tanks considering fluid-structure-soil interaction, Journal of Fluid and Structure 2006 22, 421-439.

[35] Uraz RA., Sloshing impact in roofed tanks, https://inis.iaea.org/collection/NCLCollectionStore/_Public/27/048/27048594.pdf

[36] Lu D, Zeng X, Dang J, Liu Y. A calculation method for the sloshing impact pressure imposed on the roof of a passive water storage tank of AO1000. Science and Technology of Nuclear Installations, 2016, 2016, 1-9.

[37] EN 1998-4: 2006 Eurocode 8. Design of structures for earthquake resistance. Part 4: Silos, tanks and pipelines. CEN, Brussels, 2006.